Electrochemical determination of 4-bromophenoxyacetic acid based on eGr/CeO2 composite

Haijun Du
Guizhou Minzu Univeristy
Yan Zhang
Guizhou Minzu Univeristy
Xin Wang
Guizhou Minzu Univeristy
Huali Hu
Guizhou Minzu Univeristy
Jixing Ai
Guizhou Minzu Univeristy
Huanxi Zhou
Guizhou Minzu Univeristy
Yang Yang (y.yang@gzmu.edu.cn)
Guizhou Minzu Univeristy

Research Article

Keywords: Plant growth regulators, 4-bromophenoxyacetic acid, Electrochemical determination, Lowest detection limit, eGr/CeO2 composite

Posted Date: April 7th, 2022

DOI: https://doi.org/10.21203/rs.3.rs-1509194/v1

Abstract

Plant growth regulators determination is of great importance for crops quality monitoring. In this work, 4-bromophenoxyacetic acid (4-BPA), one of the phenoxyacetic acid, is detected via electrochemical method for the first time. eGr/CeO_2 composite was constructed for the sensing materials due to the synergistic effect of excellent catalytic active sites of CeO_2 and good electron transference of electrochemical exfoliated graphene (eGr). The designed eGr/CeO_2 sensor has the active surface area of 0.097cm^2 and the roughness factor of 2.425. The eGr/CeO_2 sensor displayed a good linearity in a wide range from 0.3 to 150 μmol/L and the lowest detection limit is 0.06 μmol/L for 4-BPA detection. Electrochemical determination for 4-BPA is following a diffusion-controlled process on eGr/CeO_2 electrode, which involves 2e in the transference processes. This developed eGr/CeO_2 sensor has excellent stability with the relative standard deviation (RSD) of 2.35% in 10 continuous measurements, and good reproducibility with RSD of 3.6% in six replicated measurements. Moreover, the recoveries are in the range of 90% – 108% for detecting the 4-BPA in apple juice. The proposed eGr/CeO_2 sensor shows a great potential for plant growth regulators detecting in corps.

Introduction

Plant growth regulators (PGRs) are widely used to promote crop productivity and quality (Bons 2019; Kahlina 2021), control crop type (Wei 2013), resist biotic and abiotic stress (Fan 2020), regulate differentiation of cells, control weeds (Brondi 2005), and phytoremediation (Rostami 2019). 4-bromophenoxyacetic acid (4-BPA) is one of the PGRs, which can control weeds, accelerate plant growth, and enhance fruit setting rate. However, inappropriate usage will cause malformations and affect the quality of the crops, further, the accumulation in the crops will detriment to other plants, animals and human health. Therefore, it is necessary to develop convenient, sensitive and reliable analytical methods for 4-BPA determination. Unfortunately, only Cui group (Sutcharitchan 2020) has developed liquid chromatography-tandem mass spectrometry (LC-MS) for 4-BPA determination in Chinese herbs as we known.

4-BPA is one of the phenoxyacetic acid, and a variety of analytical methods for phenoxyacetic acid detection have been developed, including capillary electrophoresis with laser-induced fluorescence (CE-LIF) (Chen 2011), ultra-high liquid chromatography-mass spectrometry (UHPLC-MS) (Jiang 2020), headspace gas chromatography-high-performance liquid chromatography (GC-HPLC) (Qin 2018), electrochemical methods (Arduini 2019; Fusco 2017; Liu 2019; Skrzypczyńska 2016; Wang 2018). Compared to these methods, electrochemical methods have the advantages of high sensitivity, low cost, portability and simple operation (Arvand 2017; Su 2017). Because of its electrochemical activity, 4-BPA is detectable via electrochemical methods.

Ceria (CeO_2) is an n-type semiconductor that has potential using as sensing materials since it has excellent redox features, high catalytic, biocompatible, and non-toxicity (Kim 2012; Wang 2011).

Moreover, CeO_2 could selectively binding with organic molecules due to the characteristics of oxygen vacancies, free electrons, and high chemical steadiness (Ansar 2021). However, it is hard to apply directly as modifier material in electrochemical sensor due to CeO_2 suffers from poor water solubility, poor conductivity and easy aggregation. Therefore, it is very essential to enhance the sensing activities by introducing conductive support. Graphene (Gr) is one of the best candidates as it has unique and extraordinary two-dimensional (2D) honeycomb crystal structure and excellent material properties, such as high carrier mobility, high specific surface area, high electrical conductivity (Chen 2015; Sun 2019). In the study of Liu (2016), gold-palladium nanoparticles were casted on the graphene nano-platelets, and the nanocomposites show high electrocatalytic ability towards oxidation of hydrazine. Li (2019) synthesized three kinds of CeO_2 nanostructures and then loaded on the graphene nanoplatelets to detect phenolic pollutants, which exhibited excellent electrochemical activity. Previously, our group has developed electrochemical exfoliation graphene (eGr) sensor, which displays a lowest detection limit (LOD) of 0.15 μM for electrochemical determination of Kinetin (Zhang 2022). Therefore, eGr was employed as supporter to load CeO_2 to form the nanocomposite that will play synergetic effect between Gr and CeO_2, thus forming a sensitive, selective and promising electrode system for 4-BPA detection.

Herein, we firstly synthesized CeO_2 nanocubics via hydrothermal method. Highly accessible surface area and good electrical conductivity graphene was prepared by means of electrochemical exfoliation method (Zhang 2022), which was selected as the supporter to load CeO_2 nanomaterial. Then, eGr and CeO_2 composite were constructed and employed to detect 4-BPA for the very first time (Fig. 1). The developed eGr/CeO_2 sensor has a linear range from 0.3 to 150 μM and the LOD is 0.06 μM for 4-BPA determination, which shows a great potential for plant regulators detection.

Experimental

2.1 Reagents and materials

All reagents used in the experiments are analytical reagent grade and without any treatment. Graphite sheets were purchased from local electronic market. $Ce(NO_3)_3•6H_2O$, 4-BPA, indole 3-acetic acid, naphthalene acetic acid, 6-benzylaminopurine were purchased from Macklin biochemical Technology Co., Ltd. (Shanghai China). A solution of 0.1 M 4-BPA was prepared by dissolving a suitable amount of 4-BPA in alcohol and diluting the mixture to 10 mL, then the solution was stored in a refrigerator at 4 ℃. Phosphate buffer solution (PBS) was used as supporting electrolyte by combining a stock solution of 0.1 M KH_2PO_4 and 0.1 M NaH_2PO_4, then 0.1 M H_3PO_4 and 0.1 M NaOH were respectively used to adjust the pH to desire value.

2.2 Preparation of CeO_2, eGr and CeO_2/eGr composites

CeO_2 nanocubic was prepared by hydrothermal method. Firstly, 0.6948 g $Ce(NO_3)_3•6H_2O$ and 0.0224 g hexamethylenetetramine (HMT) were dissolved in 40 mL distilled water and 40 mL ethanol. The resulting solution was vigorous stirred for 20 min at room temperature, then it was transferred into a 100 mL

Teflon-lined stainless-steel autoclave, and hydrothermally heated at 180 ℃ for 20 h. After that, the product was collected by centrifuging, and alternatively washed with distilled water and ethanol to pH neutral, and then dried in an oven at 80 ℃ for 12h. Finally, the obtained yellow powder was calcined at 400 ℃ for 5 h.

For eGr preparation, two electrodes cell was used including graphite foil as an anode, a platinum net as cathode, and 0.1 M NH_4SO_4 as supporting electrolyte. Whereas, the eGr was obtained with the aid of SO_4^{2-} intercalation and oxidization to produce sulfur dioxide and oxygen gases, then the product was centrifuged, filtrated and dried overnight.

9 mg CeO_2 and/or 9 mg eGr were dispersing in 9 mL *N, N*-dimethylformamide (DMF) solution and obtained stable CeO_2, eGr, and eGr/CeO_2 suspensions with vigorous stirring and then ultra-sonicating for 2 h. The glass carbon electrodes (GCEs) were polishing to a mirror-like surface with 0.3 and 0.5 μm Al_2O_3 slurries on chamois leather, followed by rinsing with distilled water/ethanol (1:1, v/v) and double distilled water for 3 min. Finally, CeO_2, eGr, and eGr/CeO_2 suspensions were respectively drop-coating on the mirror-like surface of GCEs to obtain CeO_2/GCE, eGr/GCE, and eGr/CeO_2/GCE.

2.3 Characterization

Scanning electron microscope (SEM, Thermo scientific Apreo 2C) and transmission electron microscope (TEM) and High-resolution transmission electron microscope (HRTEM, FEI Tecnai F20, TF30) were using to analyze the surface morphologies of CeO_2, eGr and eGr/CeO_2 nanocomposite. Raman spectra data were obtained by a Thermo FisherDxr2xi Raman spectroscopy with a 532 nm diode laser. X-ray diffraction (XRD) patterns were recorded by PANayltical Empyrean system. X-ray photoelectron spectra (XPS) were recorded by Thermo Scientific K-Alpha.

Cyclic voltammetry (CV), linear sweep voltammetry (LSV), and differential pulse voltammetry (DPV) measurements were performed on a CHI 660E electrochemical workstation (Shanghai Chenhua Instrument Co.Ltd.) and classically three-electrode system. A glassy carbon electrode (GCE, diameter 3mm) or modified GCE as working electrode, a platinum wire served as counter electrode and Ag/AgCl used as reference electrode.

2.4 Sample pretreatment

The purchased apple was squeezed into juice (120 g) and the freshly apple juice was mixed with distilled water, and sonicated for 20 min (at room temperature), then centrifuged 5 min with 10000 r/min to obtain the supernatants. Supernatants were collected for further quantification of 4-BPA.

Results And Discussion

The morphologies of CeO_2/eGr, CeO_2, and eGr were observed by SEM and TEM. The eGr/CeO_2 nanocomposite used here was 1:1 in weight ratio (1:1 wt.). From Fig. 2a, it shows that CeO_2 uniformly

loaded on the surface of eGr, and the corresponding elemental mapping (Fig. 2b, c, d **and e**) illustrated the elements of C, O and Ce are existed in CeO_2/eGr nanocomposite. From Fig. 2f, the synthesized CeO_2 presents nano-cubic structure and agglomerated together due to the nanosize effects. The diffraction rings in the selected area electron diffraction (SAED) suggests the as-synthesized CeO_2 is polycrystalline and mainly exists (111), (200), (220) and (311) crystallite planes (Fig. 2g). The lattice space distance of 0.314 nm belongs to (111) crystallite plane of CeO_2 (Fig. 2h). The eGr displays layered structure (Fig. 2i), and SAED indicates that the eGr mainly presents (002), (004) crystallite planes (Fig. 2j), the lattice space distance of 0.34 nm is the theoretical value of graphene (002) crystallite plane, it verifies the high quality of the prepared eGr.

The crystallite structure and composition of CeO_2, eGr and eGr/CeO_2 composite (1:1 wt.) were evaluated by Raman spectra, XRD and XPS. In Raman spectra of Fig. 3a, it shows a characteristic peak located at 461 cm^{-1} for CeO_2 sample, which stems from the symmetrical stretching of Ce-O vibrational and originates from the F2g vibrational mode of CeO_2 phase (Tan 2015). For eGr, the peaks at 1356, 1580 and 2710 cm^{-1} were assigned to D, G and 2G bands of graphene, respectively (Yu 2018). The D band at ~ 1356 cm^{-1} is deriving from the defects and structural disorder in the sp^2-carbon nanomaterials. The G band at 1580 cm^{-1} is relating to the in-plane vibrations of the 2D hexagonal graphene lattice. eGr/CeO_2 composite sample possesses both Raman characteristics of CeO_2 and eGr. XRD was using to analyze the structure of the prepared materials. In Fig. 3b, the strong and sharp diffraction peaks indicate all the samples are in good crystallinity. For eGr, two diffraction peaks at 26.4°and 54.5° are observed, which related to (002) and (004) planes of graphene, this is in accordance with the SEAD result (Fig. 2j). For CeO_2, the diffraction peaks located at 28.5°, 33.1°, 47.5°, 56.3°, 59.1°, 69.4°, 76.7°, 79.1°and 88.4° are corresponding to (111), (200), (220), (311), (222), (400), (331), (420), (422) planes (JCPDS 81–0792). The eGr/CeO_2 composite contains all the characteristic peaks of CeO_2 and eGr as well. Base on the eGr/CeO_2 composite contains all the features of CeO_2 and eGr, the chemical composition of eGr/CeO_2 composite was further characterized by XPS. The XPS survey spectrum (Fig. 3c) reveals the existence of Ce, O, C elements in eGr/CeO_2 composite. The Ce3d electron core line was analyzed and depicted in Fig. 3d, it can be deconvoluted into 8 peaks and labeled as v0, v1, v2, v3 ($3d_{3/2}$ region) and u0, u1, u2, u3 ($3d_{5/2}$ region). Peaks v0, v2, v3 and u0, u2, u3 are characteristics of Ce(IV) 3d final states, while, v1 and u1 are Ce(III) 3d final states (Mullins 1998). Therefore, the as-prepared CeO_2 contains part of Ce(III), and the percentage of Ce(III) was calculated by Eq. (1), which based on the fitted areas of the corresponding peaks of Ce(III) and Ce(IV).

$$\left(Ce^{3+}\right)_{surf} = \frac{Ce(III)}{Ce(III) + Ce(IV)}$$

1

The calculated percentage of Ce(III) is ~ 20%, which is similar to the previous reported CeO_2 nanomaterials (Lyu 2022). The presence of Ce(III) indicates that the formation of oxygen vacancies,

which can provide catalytically active sites for the sensor. The O1s spectrum can be separated into three peaks and illustrated in Fig. 3e, the peak locates at ~ 529.9 eV corresponding to the crystal lattice oxygen in Cerium oxide CeO_2. The peak located 532.2 eV and 533.4 eV could be respectively related to the oxygen vacancy and the adsorbed oxygen on the composite (Meng 2013; Yang 2014). The C1s spectrum can be separated into three peaks (Fig. 3f). The peak placed at 284.6 eV corresponds to the sp2 carbon atoms or attribute to C = C (Parvez 2014). The other small peaks at 286.1 and 287.9 eV correspond to C–O and C = O on the surface of the composite, respectively.

The prepared eGr, CeO_2 and eGr/CeO_2 composite (1:1 wt.) were respectively casted on glass carbon electrode (eGr/GCE, CeO_2/GCE and eGr/CeO_2/GCE), and their electrochemical performances were firstly estimated by Cyclic voltammetry (CV) at 50 mV s^{-1} in the solution of 5 mM $[Fe(CN)_6]^{3-/4-}$ and 0.1 M KCl. The bare GCE electrode was conducting as control sample. From Fig. 4a, all electrodes show different levels of electrochemical activities, after evaluated the redox peak current densities and CV curve area, the electrochemical activity follows the order of eGr/CeO_2/GCE > CeO_2/GCE > eGr/GCE > GCE. This suggests that the eGr/CeO_2/GCE has the largest specific surface area, the best electrochemical kinetics and activities, which could arise from the synergistic effects of excellent catalytic active sites of CeO_2 and good electron transference of eGr. In addition, the standard heterogeneous rate constant (k^0) for bare GCE, eGr/CeO_2/GCE, eGr/GCE, CeO_2/GCE were calculated by Nicholson's equation (Nicholson 1965) and the values are respectively 0.0041 cm·s^{-1}, 0.0077 cm·s^{-1}, 0.0045 cm·s^{-1}, 0.0049 cm·s^{-1}. The eGr/CeO_2/GCE has the highest value of 0.0077 cm s^{-1} that verifies eGr/CeO_2 composite has the best electrochemical activity.

The electro-active surface area is a critical factor for electrochemical sensor, which was estimated in $[Fe(CN)_6]^{3-/4-}$ solution with scan rates ranging from 0.03 to 0.45 V s^{-1} via Randles-Sevcik equation (Eq. (2)) (Sha 2019).

$$I_{\mathrm{pa}} = (2.69 \times 10^5) n^{3/2} A D^{1/2} C v^{1/2}$$

2

Where n refers to electron transfer number, A is the active surface area, *C* is the concertation of $[Fe(CN)_6]^{3-/4-}$, *v* is the scan rate and D is the diffusion coefficient. Here, n = 1, D = $6.6 \cdot 10^{-6}$ cm^2 s^{-1} [27] for 5 mM $K_3[Fe(CN)_6]$ solution containing 0.1 M KCl. For eGr/CeO_2/GCE (Fig. 4b), the active surface area of eGr/CeO_2/GCE was calculated to be 0.097cm^2 (Fig. 4c), which is the highest than that of the electroactive surface areas of GCE (0.04 cm^2), eGr/GCE (0.08 cm^2), and CeO_2/GCE (0.065 cm^2), which displayed in **Supporting Information**, **Fig. S1**. This result agrees well with the electrochemical activity order of the prepared sensors. The roughness factor (f_r) of the electrochemical sensors was calculated to evaluate the actual active surface area by comparing the oxidation peak current (I_{pa}) of the prepared sensor to bare GCE for $[Fe(CN)_6]^{3-/4-}$ reaction (Krzyczmonik 2014). The ratio of the oxidation peaks current for two electrodes is equal to the electrode surface area (Eq. (3)):

$$f_r = \frac{I_{P2}}{I_{P1}} = \frac{A_2}{A_1}$$

3

The f_r determined by electrochemical methods depends not only on the size of the electrode (the actual surface), but also on the number of redox centers that can be reached on the surface. Therefore, the f_r was calculated to 2.425, 2, and 1.625 for eGr/CeO_2/GCE, eGr/GCE, and CeO_2/GCE, respectively.

The GCE, eGr/GCE, CeO_2/GCE and eGr/CeO_2/GCE (1:1 wt.) for 4-BPA detection were characterized by CV in the electrolyte of absence and presence 50 μmol L^{-1} 4-BPA in 0.1 mol L^{-1} phosphate buffer (pH = 3). As displayed in Fig. 5a, when presence 50 μmol L^{-1} 4-BPA, all electrodes present one oxidation peak, which indicates the 4-BPA is electrochemically detectable and the reaction of 4-BPA is irreversible. The eGr/CeO_2/GCE (1:1 wt.) shows the highest oxidation peak current (I_{pa}) and the lowest onset potential, this verified that eGr/CeO_2 composite has higher sensitivity for electrochemical detection of 4-BPA, which should be attributed to the synergetic effect of the catalytic properties of CeO_2 and the fast electron transference of eGr. The ratios between CeO_2 and eGr have further been measured and shown in Fig. 5b. With CeO_2: eGr ratio increasing from 0:4 to 1:1, the oxidation peak current of 4-BPA increases and reaches the maximum at the ratio of 1:1, then the peak current drops with further increasing CeO_2 content. The reason could be CeO_2 is a semiconductor, and it provides electrocatalytic activity sites. When CeO_2 content is too low, and it will not create enough activity sites. While the content is higher than 1: 1, the conductivity and electron transference of the electrode will decrease. Therefore, the optimum ratio was 1: 1 for 4-BPA detection and selected in the following study.

The different loading amounts of eGr/CeO_2 composite on GCE were measured with 10 μmol L^{-1} 4-BPA **(Supporting information**, **Fig.S2)**. It found that the oxidation peak current of 4-BPA increases with the loading volume increasing to 6 μL, while the response decreased when the loading amount further increased (Fig. 5c). This could be arising from the electrode surface was not covering enough when the loading composites below 6 μL, while too much loading amount will hinder the activity sites that cause the decrease on the response peak current (Zamiri 2019).

The PBS, Britton-Robison (B-R), and acetic acid-sodium acetate buffer solutions were evaluated as supporting electrolytes for 4-BPA detection (**Supporting information**, **Fig.S3**). Among these supporting electrolytes, the PBS buffer solution shows more sensitivity for 4-BPA detection. Therefore, PBS was selected as supporting electrolyte. Moreover, pH is another key impact factor for electrochemical analysis. The pH values range from 3 to 6.5 were evaluated in 0.1 M PBS buffer solution **(Supporting information**, **Fig.S4)**. It can be seen that the optimum response pH for 4-BPA was 3, and the response gradually decreases as the pH increasing (Fig. 5d). This phenomenon could be due to the conductivity loss and presence of carboxyl groups with pH increasing (Chen 2020).

The oxidation process of 4-BPA on eGr/CeO_2/GCE was further studied by linear sweep voltammograms (LSVs), different scan rates (50 mV s^{-1} to 450 mV s^{-1}) were conducted and 20 μmol L^{-1} 4-BPA was used. As exhibited in Fig. 6a, the I_{pa} increases with scan rates increased. Moreover, the oxidation peaks positively shifted. More importantly, the oxidation peak current increased linearly with the square root of scan rates (Fig. 6b), and the linear regression is $I_{pa} = 3.936v^{1/2}-9.318$, $R^2 = 0.999$, which indicates that the electrochemical oxidation of 4-BPA on eGr/CeO_2/GCE was controlled by diffusion process (Huang 2020). The relationship between E_{pa} and ln$v$ was presented by Laviron's theory (Sequoia 1979):

$$E_{\mathrm{pa}} = E^0 + \left(\frac{RT}{\alpha nF}\right)\ln\left(\frac{RTk^0}{\alpha nF}\right) + \left(\frac{RT}{\alpha nF}\right)\ln v$$

4

where α is the charge transfer coefficient, E^0 is the apparent potential, n is the number of electron, v is the scan rate, the value of R, T, F is 8.314 J K^{-1} mol^{-1}, 298 K, 96485 C mol^{-1}, respectively. Therefore, the number of electron can be calculated via the linear equations of E_{pa} - ln$v$ (**Supporting information, Fig.S5**). Generally, for a totally irreversible electrode process, the value of α is assumed to be 0.5. Hence, the value of n is calculated to be 2.

DPV shows sensitive response to low concentrations as compared to LSV. Therefore, DPV was using to detect 4-BPA in PBS solution with different concentrations. As illustrated in Fig. 6c, the peak current increases linearly with the concentrations of 4-BPA varying from 0.3 to 150 μM. However, there are two linear relationships obtained. From Fig. 6d, in the range of 0.3 to 20 μM, the linear regression equation is $I_{pa} = 0.75c + 0.08$, ($R^2 = 0.991$), and from 20 to 150 μM, the linear relationship is $I_{pa} = 0.199c + 11.24$, ($R^2 = 0.993$). Moreover, the lowest detection limit (LOD) was calculated to be 0.06 μmol L^{-1} according to the following equation of 3s/m, where m is slope of the regression equation and s is the stand deviation of the response.

The repeatability of the eGr/CeO_2/GCE was carried out with 10 μmol L^{-1} 4-BPA by the means of LSV (**Supporting information, Fig.S6**). After 10 continuous measurements (**Fig.S7a**), the relative standard deviation (RSD) of the oxidation peak currents was found to be 2.35% for 4-BPA. After storing the electrode at 4 ℃ for 15 days, the electroactive oxidation of 4-BPA was just reducing 3.21% compared to the original currents. To investigate the reproducibility of the sensor, six replicated measurements for 10 μmol L^{-1} 4-BPA were carried out using 7 different eGr/CeO_2/GCEs that made same method and same materials. The results showed excellent reproducibility with relative standard deviations of 3.6%. These results indicate that the proposed sensor has good repeatability and reproducibility.

To estimate the ability of anti-interference of the eGr/CeO_2/GCE, some regular interfering species were tested. From **Fig.S7b**, no considerable interferences were observed from the following compounds: K^+, Na^+, Mg^{2+}, rutin, quercetin, fenitrothion, imidacloprid, clothianidin, IAA, SA, glucose, sucrose (peak current

change < 6%). However, when adding the homologs of phenoxyacetic acid (4-chlorophenoxyacetic acid, 4-fluorophenoxyacetic acid), there exist some interferences. Therefore, we need to explore more sensitive, stable materials to solve the problem in the future study.

To evaluate the practicability of eGr/CeO_2/GCE, the sensor was using to detect 4-BPA in real apple samples. It was found that no response of 4-BPA in the apple sample, and the recoveries were then evaluated by standard addition method and the analytical results are listed in Table 1.

Table 1
Results of the recovery analysis of 4-BPA in apple sample (n = 3)

Sample	Added value(μM)	Determined value(μM)	Recovery(%)
1	0	Not detected (a, b)	-
2	0.5	0.45 ± 0.01	90%
3	1	1.08 ± 0.04	108%
4	3	2.78 ± 0.03	93%
5	5	4.86 ± 0.04	97%
a The 4-BPA level determined by proposed eGr/CeO_2/GCE			
b The 4-BPA level determined by HPLC system			

Conclusion

In this work, we constructed a selective, sensitive electrochemical method based on eGr/CeO_2 composite modified GCE to electrochemically detect the plant growth regulator of 4-BPA. The prepared eGr/CeO_2 sensor exhibits excellent electrocatalytic activity with the active surface area of 0.097cm^2 and the roughness factor of 2.425. The best pH is 3 and the optimized ratio of CeO_2 : eGr is 1:1 for 4-BPA determination. The eGr/CeO_2 sensor exhibited a good linearity in a wide range from 0.3 to 150 μmol/L and a lowest detection limit of 0.06 μmol/L for 4-BPA detection. Electrochemical oxidation of 4-BPA is following diffusion-controlled process, which involves 2 e in the transference processes. In addition, there were no significant interfering substances among K^+, Na^+, Mg^{2+}, rutin, quercetin, fenitrothion, imidacloprid, clothianidin, IAA, SA, glucose, sucrose. The proposed electrochemical sensor shows excellent repeatability with the RSD of 2.35% for 10 measurements and great reproducibility with the RSD of 3.6% for 7 electrodes. The low cost and easy made sensor have a great potential for detecting other plant growth regulators.

Declarations

Acknowledgements

This research was supported by the National Natural Science Foundation of China (No. 51801039, 81860701, 82060714), Natural Science Foundation of Guizhou Province, China (NO. ZK [2021]242).

Funding declaration

This work was financially funded by the National Natural Science Foundation of China (No. 51801039, 81860701, 82060714), Natural Science Foundation of Guizhou Province, China (NO. ZK [2021]242). The funding source did not have any involvement in experiment design, in data collection, analysis and interpretation, and in manuscript writing and submitting for publication.

Conflict of interest

The authors declare no conflict of interests.

Author contribution

Y.Y. conceived the idea and advised the study, H.D and Y. Z. wrote the main manuscript and conducted the experiment, X.W. prepared the CeO_2 samples. H. H. and J. A. prepared the figures 3-5, H.Z. conducted the XRD and Raman tests. All authors reviewed the manuscript.

Data availability statement

The authors confirm that the data supporting the findings of this study are available within the article and/or its supplementary materials.

References

1. Arvand M, Gaskarmahalleh A A, Hemmati S, (2017) Enhanced-Oxidation and Highly Sensitive Detection of Tartrazine in Foodstuffs via New Platform Based on Poly(5-Sulfosalicylic Acid)/$Cu(OH)_2$ Nanoparticles. Food Anal Methods 10: 2241–2251.
2. Arduini F, Cinti S, Caratelli V et al (2019) Origami multiple paper-based electrochemical biosensors for pesticide detection. Biosens Bioelectron 126: 346–354.
3. Ansari A A, Alam M (2021) Nickle-ion-substituted ceria nanoparticles-based electrochemical sensor for sensitive detection of thiourea. J Mater Sci 32: 23266–23274.
4. Brondi S H G, Lanças F M (2005) Development and validation of a multi-residue analytical methodology to determine the presence of selected pesticides in water through liquid chromatography. J Braz Chem Soc 16: 650–654.
5. Bons H K, Kaur M (2019) Role of plant growth regulators in improving fruit set, quality and yield of fruit crops: a review. J Hortic Sci Biotechnol 95(2): 137–146.
6. Chen H, Feng X, Guo H S et al (2011) Simultaneous determination of phytohormones containing carboxyl in crude extracts of fruit samples based on chemical derivatization by capillary

electrophoresis with laser-induced fluorescence detection. J Chromatogr B 879(20): 1802–1808.

7. Chen C H, Yang S W, Chuang M C et al (2015) Towards the continuous production of high crystallinity graphene via electrochemical exfoliation with molecular in situ encapsulation. Nanoscale 7: 15362–15373.
8. Chen Y N, Chen Q, Zhao H et al (2020) Wheat Straws and Corn Straws as Adsorbents for the Removal of Cr(VI) and Cr(III) from Aqueous Solution: Kinetics, Isotherm, and Mechanism. ACS Omega 5(11): 6003–6009.
9. Fusco G, Gallo F, Tortolini C et al (2017) AuNPs-functionalized PANABA-MWCNTs nanocomposite-based impedimetric immunosensor for 2,4-dichlorophenoxy acetic acid detection. Biosens Bioelectron 93: 52–56.
10. Fan Y X, Yang W, Yan Q Q et al (2020) Genome-Wide Identification and Expression Analysis of the Protease Inhibitor Gene Families in Tomato. Genes 11(1): 1.
11. Huang Q, Lin X, Tong L et al (2020) Graphene Quantum Dots/Multiwalled Carbon Nanotubes Composite-Based Electrochemical Sensor for Detecting Dopamine Release from Living Cells. ACS Sustainable Chem Eng 8: 1644–1650.
12. Jiang C L, Dai J X, Han H L et al (2020) Determination of thirteen acidic phytohormones and their analogues in tea (Camellia sinensis) leaves using ultra high performance liquid chromatography tandem mass spectrometry. J Chromatogr B 1149: 122144.
13. Kim C K, Kim T, Choi I Y et al (2012) Ceria Nanoparticles that can Protect against Ischemic Stroke. Angew. Chem Int Ed Eng 51(44): 11039–11043.
14. Krzyczmonik P, Socha E, Skrzypek S et al (2014) Honeycomb-structured porous poly(3,4-ethylenedioxythiophene) composite layers on a gold electrode. Thin Solid Films 565: 54–61.
15. Kahlina K V, Jurić S, Marijan M et al (2021) Synthesis, Characterization, and Encapsulation of Novel Plant Growth Regulators (PGRs) in Biopolymer Matrices. Int J Mol Sci 22(4): 1847.
16. Liu Y, Qiu Z P, Wan Q J et al (2016) High-Performance Hydrazine Sensor Based on Graphene Nano Platelets Supported Metal Nanoparticles. Electroanalysis 28(1): 126–132.
17. Liu F P, Qin X W, Huang Z F, (2019) Green synthesis of porous graphene and its application for sensitive detection of hydrogen peroxide and 2,4-dichlorophenoxyacetic acid. Electrochim Acta 295: 615–623.
18. Li C, Zhang Y Y, Zeng T et al (2019) Graphene nanoplatelet supported CeO_2 nanocomposites towards electrocatalytic oxidation of multiple phenolic pollutants. Anal Chim Acta 1088: 45–53.
19. Lyu L, Xie Q, Yang Y Y et al (2022) A Novel CeO_2 Hollow-Shell Sensor Constructed for High Sensitivity of Acetone Gas Detection. Appl Surf Sci 571: 151337.
20. Mullins D R, Overbury S H, Huntley D R (1998) Electron spectroscopy of single crystal and polycrystalline cerium oxide surfaces. Surf Sci 409(2): 307–319.
21. Meng F M, Wang L N, Cui J B (2013) Controllable synthesis and optical properties of nano-CeO_2 via a facile hydrothermal route. J Alloys Compd 556: 102–108.

22. Nicholson R S (1965) Theory and Application of Cyclic Voltammetry for Measurement of Electrode Reaction Kinetics. Anal Chem 37: 1351–1355.
23. Parvez K, Wu Z S, Li R et al (2014) Exfoliation of Graphite into Graphene in Aqueous Solutions of Inorganic Salts. J Am Chem Soc 136(16): 6083–6091.
24. Qin G F, Zou K T, Tian L et al (2018) Determination of Five Plant Growth Regulator Containing Carboxyl in Bean Sprouts Based on Chemical Derivatization by GC-MS. Food Anal Methods 11: 2628–2635.
25. Rostami S, Azhdarpoor A (2019) The application of plant growth regulators to improve phytoremediation of contaminated soils: A review. Chemosphere 220: 818–827.
26. Sequoia E, Laboratoire O N, Organique P et al (1979) General expression of the linear potential sweep voltammogram in the case of diffusionless electrochemical systems. J Electroanal Chem 101: 19–28.
27. Skrzypczyńska K, Kuśmierek K, Świątkowski A (2016) Carbon paste electrodes modified with various carbonaceous materials for the determination of 2,4-dichlorophenoxyacetic acid by differential pulse voltammetry. J Electroanal Chem 766: 8–15.
28. Su D D, Zhang Y Y, Wang Z J et al (2017) Decoration of graphene nano platelets with gold nanoparticles for voltammetry of 4-nonylphenol. Carbon 117: 313–321.
29. Sun J J, Xie X H, Xie K et al (2019) Magnetic Graphene Field-Effect Transistor Biosensor for Single-Strand DNA Detection. Nanoscale Res Lett 14: 248.
30. Sha T, Liu J, Sun M et al (2019) Green and low-cost synthesis of nitrogen-doped graphene-like mesoporous nanosheets from the biomass waste of okara for the amperometric detection of vitamin C in real samples. Talanta 200: 300–306.
31. Sutcharitchan C, Miao S, Li W T et al (2020) High performance liquid chromatography-tandem mass spectrometry method for residue determination of 39 plant growth regulators in root and rhizome Chinese herbs. Food Chem 322: 126766.
32. Tan H Y, Wang J, Yu S Z et al (2015) Support Morphology-Dependent Catalytic Activity of Pd/CeO_2 for Formaldehyde Oxidation. Sci Technol 49(14): 8675–8682.
33. Wang Z L, Li G R, Ou Y N et al (2011) Electrochemical deposition of Eu^{3+}-doped CeO_2 nanobelts with enhanced optical properties. J Phys Chem C 115: 351–356.
34. Wei Y Z, Zhang H N, Li W C et al (2013) Phenological growth stages of lychee (Litchi chinensis Sonn.) using the extended BBCH-scale. Sci Hortic 161: 273–277.
35. Wang H M, Xu Q, Wang J et al (2018) Dendrimer-like amino-functionalized hierarchical porous silica nanoparticle: A host material for 2,4-dichlorophenoxyacetic acid imprinting and sensing. Biosens Bioelectron 100: 105–114.
36. Yang Y, Yang Y M, Fu T W et al (2014) Influence of ethanol content in the precursor solution on anodic electrodeposited CeO_2 thin films. Thin Solid Films 556: 128–136.

37. Yu J, Zhang Y Y, Li H et al (2018) Electrochemical properties and sensing applications of nanocarbons: A comparative study. Carbon 129: 301–309.
38. Zamiri R, Salehizadeh S A, Ahangar H A et al (2019) Dielectric and optical properties of Ni- and Fe-doped CeO_2 Nanoparticles. Appl Phys A 125: 393.
39. Zhang Y, Ai J X, Hu H L et al (2022) Highly Sensitive Detection of Kinetin with Electrochemical Exfoliation of Graphene Nanosheets. Appl Phys A 128: 350.

Figures

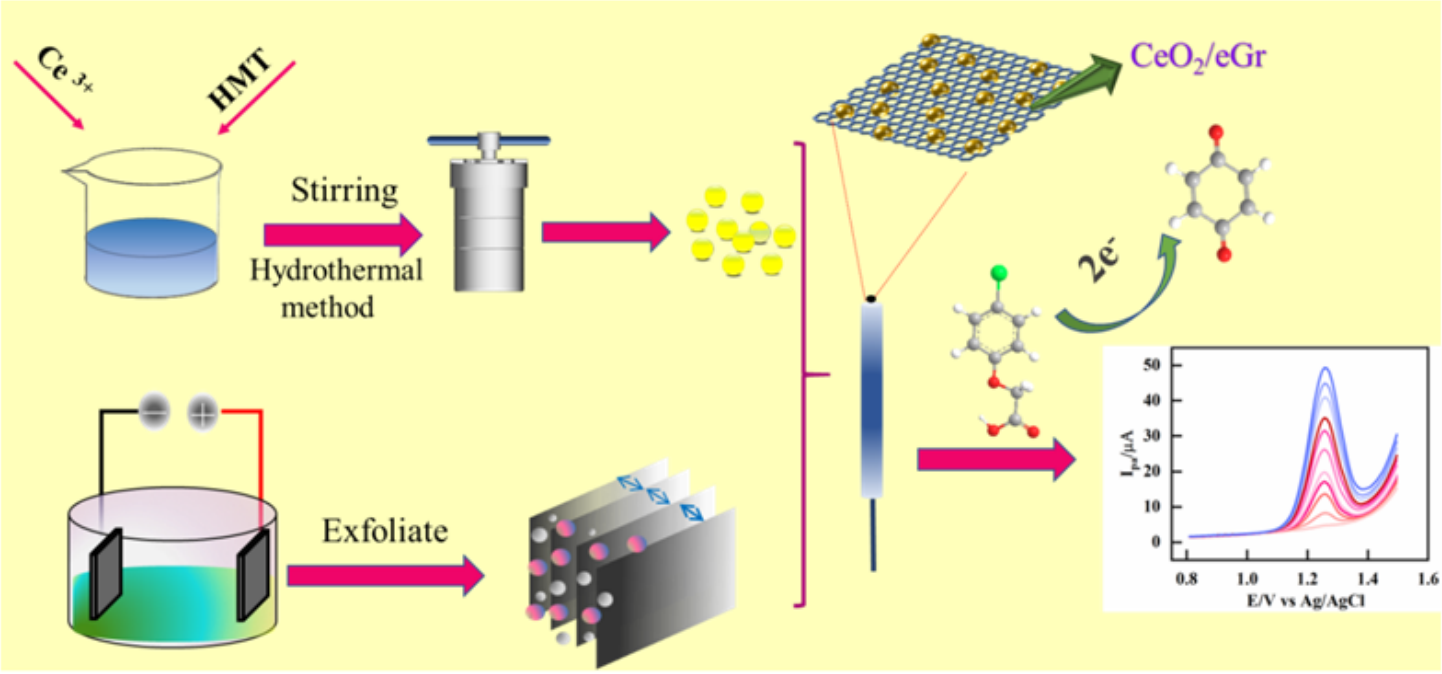

Figure 1

Scheme illustration of 4-BPA detection with eGr/CeO_2 composite.

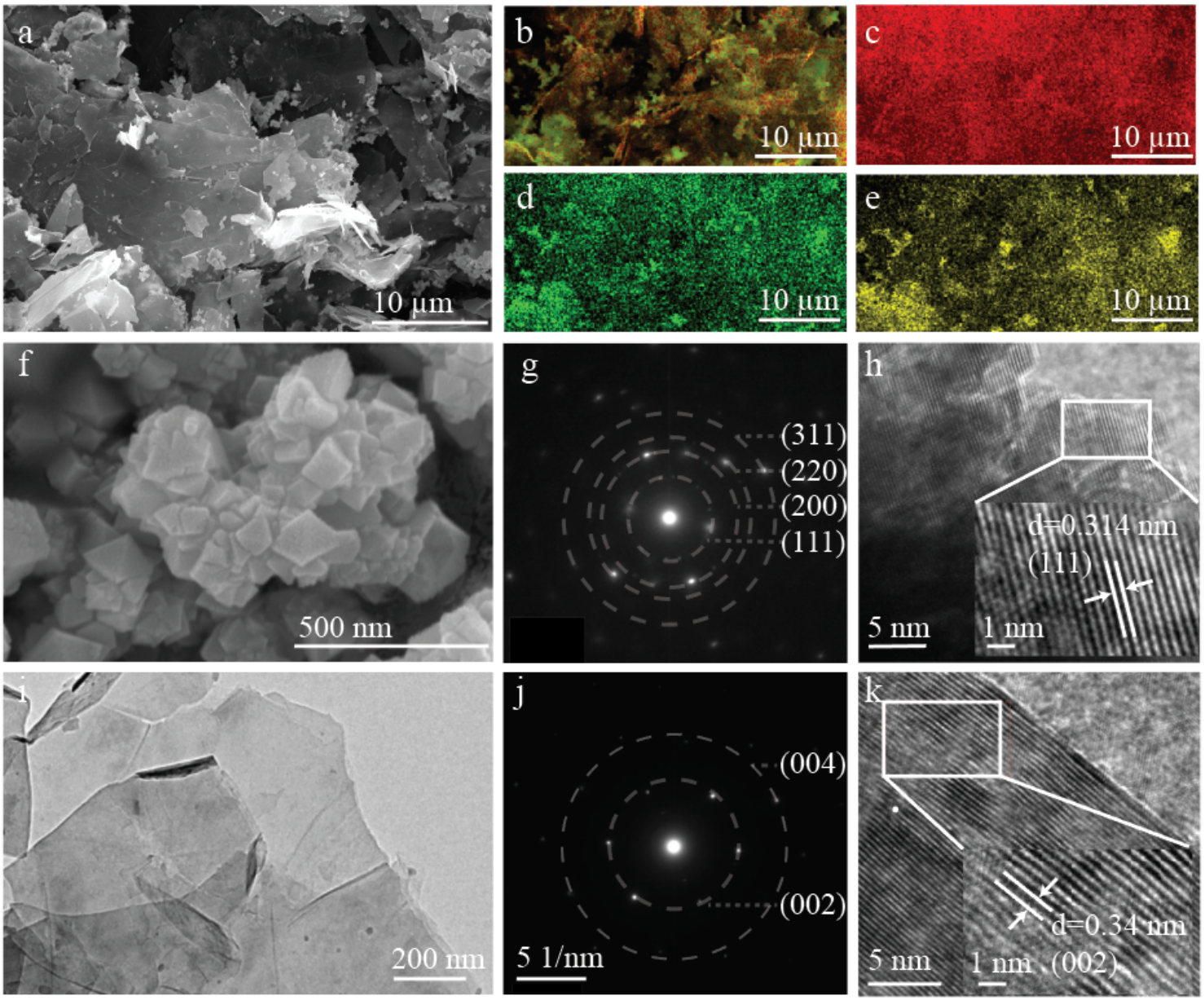

Figure 2

SEM image (a) and corresponding elemental mapping (b, c, d, e) of eGr/CeO_2, SEM image (f), SEAD (g) and HRTEM (h) of CeO_2, TEM (i), SEAD (j) and HRTEM (k) of eGr.

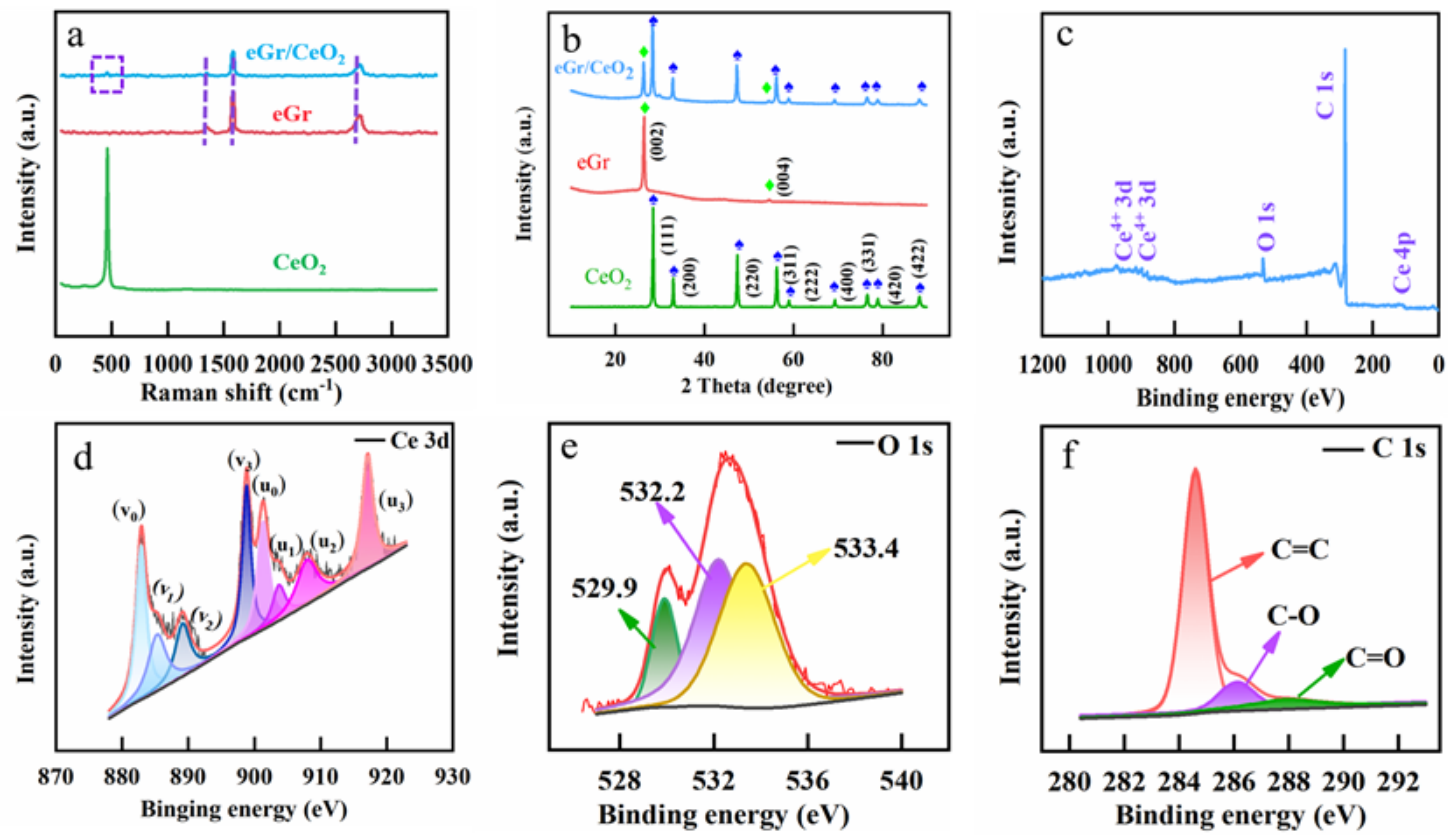

Figure 3

(a) Raman spectra, (b) XRD patterns of eGr, CeO_2, and eGr/CeO_2, (c) XPS survey spectra, (d) High resolution Ce 3d spectra, (e) O 1 s and (f) C 1s of eGr/CeO_2 composite, respectively.

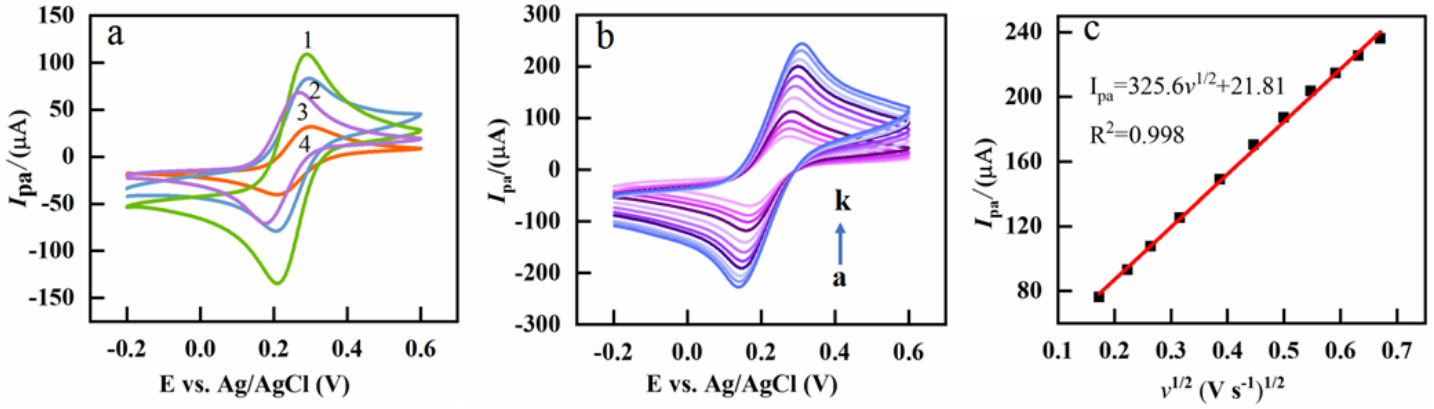

Figure 4

(a) CVs of eGr /CeO_2/GCE in the presence of 5 mM $[Fe(CN)6]^{3-/4-}$ solution in aqueous 0.1 M KCl. eGr/CeO_2/GCE (1), CeO_2/GCE (2), eGr/GCE (3), bare GCE (4); **(b)** CVs of eGr/CeO_2/GCE in the presence of

5 mM $[Fe(CN)6]^{3-/4-}$ solution in aqueous 0.1 M KCl at various scan rate (from a to k): 0.03, 0.05, 0.07, 0.1, 0.15, 0.2, 0.25, 0.3, 0.35, 0.4, 0.45 V s^{-1}. **(c)** The plot of peak currents vs. $v^{1/2}$.

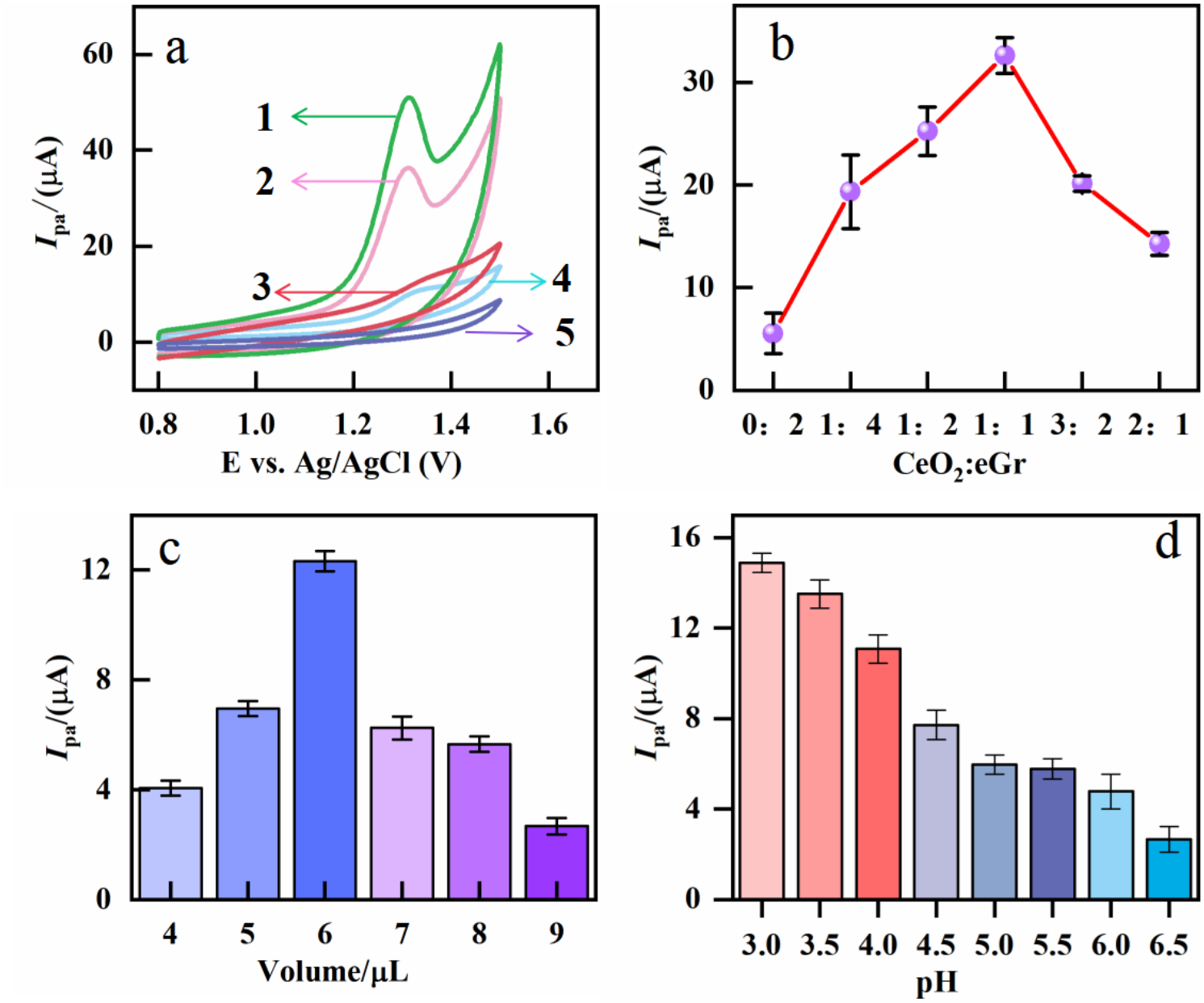

Figure 5

(a) CVs of eGr/CeO_2/GCE (1), eGr/GCE (2), bare GCE (3) and CeO_2/GCE (4) in 0.1 M PBS solution containing 50 μmol L^{-1} 4-BPA at the scan rate of 100 mV s^{-1}, blank of eGr/CeO_2/GCE (5); (b) Influence of the ratio between CeO_2 and eGr on response of 4-BPA based on LSVs. (c) the response of 10 μmol L^{-1} 4-BAP to different volumes of composite nanomaterial in PBS solution (pH=3). (d) Influence of pH on the peak current of 4-BPA in 0.1 M PBS solution.

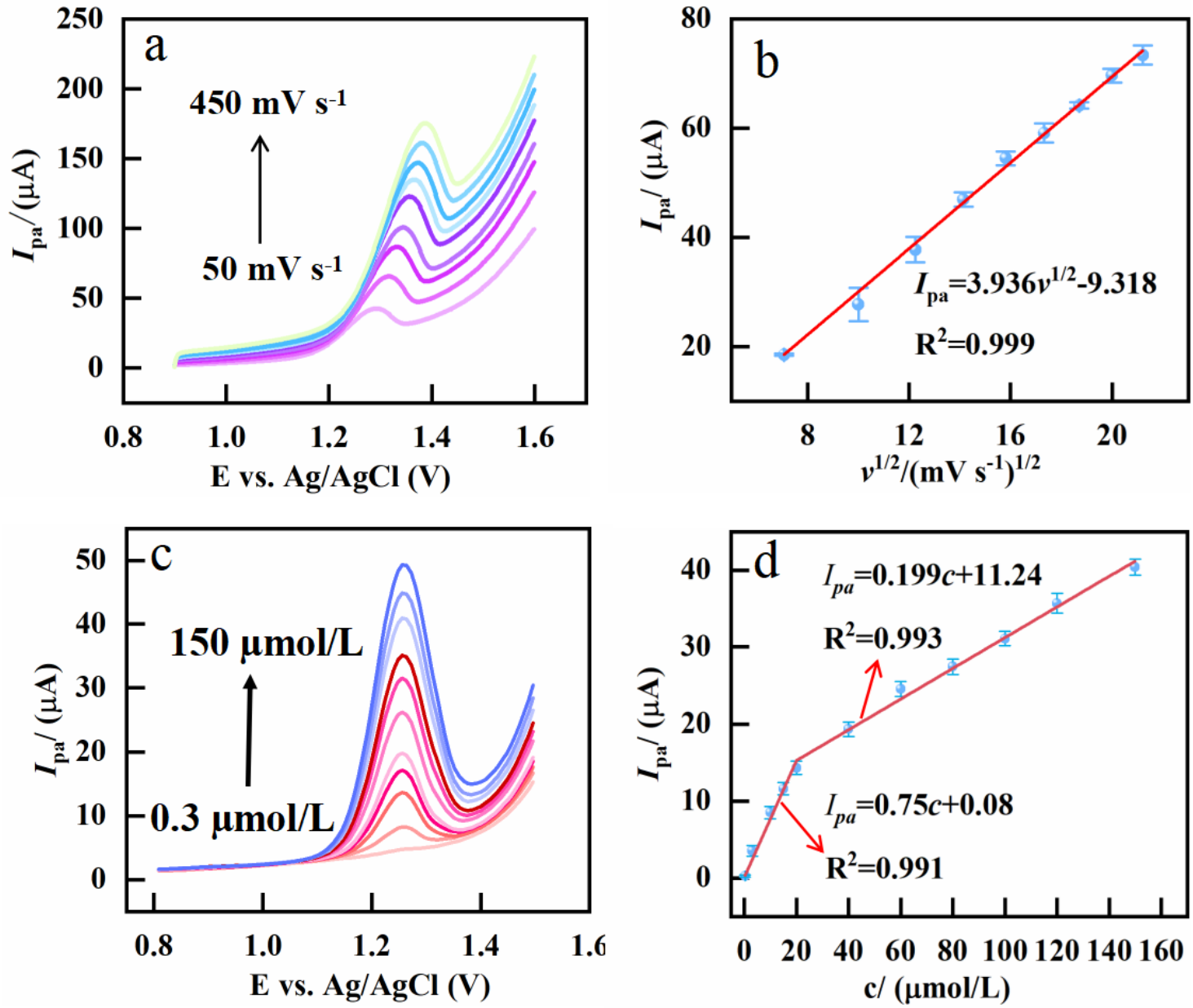

Figure 6

(a) LSVs of eGr/CeO_2/GCE in 0.1 M PBS solution containing 20 μmol L^{-1} 4-BPA at 50, 100, 150, 200, 250, 300, 350, 400, 450 mV s^{-1}, **(b)** Plots of I_{pa} vs. $v^{1/2}$, **(c)** DPVs of eGr/CeO_2/GCE in 0.1 M PBS solution containing 0.3, 3, 10, 15, 20, 40, 60, 80, 100, 120, 150 μmol L^{-1} 4-BPA, **(d)** Plots of the oxidation peak current vs. the concentration of 4-BPA.

Supplementary Files

This is a list of supplementary files associated with this preprint. Click to download.

- Supplementinformation.doc